



Published in final edited form as:

Nat Neurosci. 2015 January ; 18(1): 104–111. doi:10.1038/nn.3897.

ErbB4 regulation of a thalamic reticular nucleus circuit for sensory selection

Sandra Ahrens¹, Santiago Jaramillo^{1,†,*}, Kai Yu^{1,*}, Sanchari Ghosh¹, Ga-Ram Hwang¹, Raehum Paik¹, Cary Lai², Miao He^{1,§}, Z. Josh Huang¹, and Bo Li^{1,#}

¹Cold Spring Harbor Laboratory, Cold Spring Harbor NY 11724

²Indiana University, Bloomington, IN 47405

Abstract

Selective processing of behaviorally relevant sensory inputs against irrelevant ones is a fundamental cognitive function, impairments of which have been implicated in major psychiatric disorders. It is known that the thalamic reticular nucleus (TRN) gates sensory information en route to the cortex, however the underlying mechanisms remain unclear. Here we show in mice that deficiency of *ErbB4* gene in somatostatin-expressing TRN neurons markedly altered behaviors dependent on sensory selection. Whereas performance in identifying targets from distractors was improved, the ability to switch attention between conflicting sensory cues was impaired. These behavioral changes were mediated by enhanced cortical drive onto TRN that promotes the TRN-mediated cortical feedback inhibition of thalamic neurons. Our results uncover a previously unknown role of ErbB4 in regulating cortico-TRN-thalamic circuit function. We propose that ErbB4 sets the sensitivity of TRN to cortical inputs at levels that can support sensory selection while allowing behavioral flexibility.

The thalamic reticular nucleus (TRN) is a thin sheet of exclusively GABA (γ -aminobutyric acid)-producing neurons located between the cortex and dorsal thalamus^{1,2}. The TRN integrates both cortical and thalamic synaptic inputs, but only sends outputs to the thalamus. This unique anatomical location and connectivity have led to the proposal that the TRN controls attention through “gatekeeping” of sensory information passing through the thalamus^{1–4}. Consistent with this hypothesis, it has been shown that the activity of TRN neurons correlates with behavioral state⁵, sensory detection^{6,7}, and attention^{8–11}; and that lesions of TRN impair attentional orienting¹¹. In addition, TRN dysfunction has been implicated in schizophrenia^{2,12–14}, a mental disorder in which altered sensory processing

Users may view, print, copy, and download text and data-mine the content in such documents, for the purposes of academic research, subject always to the full Conditions of use:http://www.nature.com/authors/editorial_policies/license.html#terms

#Correspondence: Bo Li, PhD, 1 Bungtown Road, Cold Spring Harbor NY 11724, bli@cshl.edu.

†Current address: Institute of Neuroscience and Department of Biology, University of Oregon, Eugene, OR, 97403

§Current address: Institutes of Brain Science, Fudan University, Shanghai 200000, China

*These authors contributed equally to this work

AUTHOR CONTRIBUTIONS

S.A. and B.L. conceived the study. S.J., S.A., K.Y., and B.L. designed the behavioral tasks. S.A. performed the experiments with help from K.Y., S.G., G.R.H. and R.P.. S.A., S.J., and S.G. analyzed data. C.L., M.H., and Z.J.H. provided critical reagents and advice. S.A. and B.L. made figures. B.L. and S.A. wrote the manuscript with help from all authors.

The authors declare no competing financial interests.

and attentional deficit are prominent features¹⁵. Nevertheless, the cellular and synaptic mechanisms underlying TRN function remain unclear.

Recent studies suggest that the TRN may be regulated by a unique set of signaling molecules^{2,13,16,17}. For example, TRN neurons express high levels of ErbB4¹⁶, a receptor tyrosine kinase that has important roles in multiple biological processes, including neurodevelopment, neuronal excitability, and the function of excitatory and inhibitory synapses^{18,19}. Notably, ErbB4 and its ligand neuregulin-1 (NRG1) have been associated with schizophrenia and other mental disorders by human genetic studies^{18,19}. In light of these findings, as well as those that implicate TRN in attention and TRN dysfunction in mental disorders^{2,12–14,20}, it is of great interest to investigate the potential role of ErbB4 in regulating TRN circuit function in behaviors that demand sensory processing and attention.

In this study, we manipulated ErbB4 content in a major population of TRN neurons in mice, and assessed the effects on performance in novel sensory selection tasks. We observed robust behavioral effects that likely reflect changes in attention. Furthermore, by combining electrophysiological, optogenetic, and molecular techniques, we identified a critical synaptic change in the cortico-TRN-thalamic circuitry that is responsible for the ErbB4 deficiency-induced behavioral phenotypes.

RESULTS

To target ErbB4 in the TRN and establish behavioral tasks

To investigate the mechanisms underlying TRN function, we sought to use genetic techniques to selectively target TRN neurons. Given that a major TRN population expresses somatostatin (SOM)^{21,22}, we used the *Som-Cre* mice²³ that, when bred with the *Ai14* reporter mice²⁴, allow the easy identification of SOM-expressing (SOM⁺) TRN neurons (Fig. 1a–c). Previous studies indicate that TRN neurons express high levels of ErbB4^{16,18,25}. Unexpectedly, we found that ErbB4 is primarily expressed in SOM⁺ neurons in the TRN (Fig. 1b, c). In contrast, ErbB4 is largely excluded from SOM⁺ neurons in other brain areas, such as cortex and hippocampus^{26,27} (Supplementary Fig. 1, Fig. 1d). Taking advantage of this specific co-expression profile, we manipulated ErbB4 levels selectively in SOM⁺ TRN neurons by breeding the *Som-Cre;ErbB4^{lox/lox}* mice²⁸, hence generating the *Som^{ErbB4}+/-* or *Som^{ErbB4}-/-* mice (Fig. 1d).

Since the TRN is involved in sensory detection^{6,7} and attention^{8–11}, we reasoned that ErbB4 deficiency in TRN neurons might affect TRN function, thereby impairing behavioral performance that relies on sensory processing and demands attention. To test this hypothesis, we examined mice in behavioral tasks based on a two-alternative choice (2-AC) paradigm^{29,30} (Fig. 2 and Methods), which engage animals in the selection of competing sensory inputs: an “auditory/auditory” task, in which mice needed to identify the target sounds among distractor tones (Fig. 2a, c); and a “visual/auditory” task, in which mice were initially trained to respond to both sound and light cues, but in subsequent test sessions were required to respond to only the light and ignore the sound (Fig. 2a, b, and d; and Methods). The visual/auditory task contains a mix of congruent trials, in which light and sound cue the

same action, and incongruent trials in which the two stimuli cue conflicting actions (Fig. 2d).

Of note, the two behavioral tasks that we used – the auditory/auditory task and the visual/auditory task – are substantially different in two ways. First, in the former task, mice identify targets among within-modality distractors, whereas in the latter task, mice need to globally switch attention across modalities. Second, the effects of the distractors on performance in the auditory/auditory task are primarily sensory-driven (bottom-up)³¹ in nature; in contrast, the irrelevant cues (the auditory cues) in the visual/auditory task are capable of engaging in goal-directed (top-down) attention³¹, in a manner similar to the relevant cues (the visual cues), because both the auditory and visual cues were initially associated with reward during training when the mice learned the basic 2-AC tasks (Fig. 2; and Methods).

ErbB4 Deletion in SOM neurons alters sensory selection

All animals, including the $SOM^{ErbB4+/+}$ (*ErbB4* wild type, WT), $SOM^{ErbB4+/-}$ (*ErbB4* heterozygous, HET), and $SOM^{ErbB4-/-}$ (*ErbB4* knockout, KO) mice, were able to learn the basic 2-AC tasks and reach a similar performance level (Fig. 2e; Supplementary Fig. 2). Surprisingly, both HET and KO mice displayed increased performance compared with the WT in the auditory/auditory task (Fig. 3a; note 50% is chance level). It is noteworthy that the KO mice were faster in learning the basic 2-AC task than the HET and WT (Supplementary Fig. 2). Enhanced learning could therefore contribute to the increased performance in the auditory/auditory task. However, the HET mice also showed increased performance in the auditory/auditory task but had a learning curve similar to WT mice (Fig. 3a; Supplementary Fig. 2), arguing against a learning effect.

In contrast to the increased performance in the auditory/auditory task, the KO had severely impaired performance in the incongruent trials of the visual/auditory task (Fig. 3b). The HET mice showed a trend towards decreased performance that was less severe than the KO (Fig. 3b). All groups performed at similarly high levels in the congruent trials of the visual/auditory task (Fig. 3c), which do not invoke conflicting actions.

The increased performance in the auditory/auditory task and decreased performance in the incongruent trials of the visual/auditory task in the ErbB4 mutant mice could be caused by enhanced auditory perception or impaired visual perception, resulting in these mice to rely more on auditory, rather than visual cues. However, arguing against this hypothesis, the mutant mice had no obvious change in either auditory (Supplementary Fig. 3a–c) or visual (Supplementary Fig. 3d–g) perception. Furthermore, the performance of these mice was enhanced in a visual/visual task, in which they were required to identify targets among distractors in the visual field (Supplementary Fig. 4a, b); and was decreased in an auditory/visual task whereby they needed to respond to the sound cues and ignore the light cues (Supplementary Fig. 4c–e). These phenotypes mirror those observed in the auditory/auditory task and visual/auditory task, respectively (Fig. 3a–c). Thus, ErbB4 deficiency in SOM^+ neurons profoundly and differentially alters an animal's ability to select between competing sensory inputs. Whereas performance in the within-modality tasks was enhanced, performance in the across-modalities tasks was impaired.

ErbB4 Deletion in SOM TRN neurons alters sensory selection

The observed behavioral phenotypes in the $SOM^{ErbB4+/-}$ or $SOM^{ErbB4-/-}$ mice could be caused by ErbB4 deficiency in the TRN. However, although the majority of cortical or hippocampal SOM^+ neurons do not express ErbB4^{26,27}, some of them do (Supplementary Fig. 1). In addition, ErbB4-expressing SOM^+ neurons might exist in other brain areas. These neurons can potentially be affected in the ErbB4 mutant mice and therefore contribute to the behavioral phenotypes. To address this problem, we selectively deleted ErbB4 in the TRN. To this end, we bred the $Som-Flp;ErbB4^{lox/lox}$ mice, in which the flippase (Flp) is selectively expressed in SOM^+ neurons from an $ErbB4^{lox/lox}$ genetic background, and injected the TRN of these mice with an adeno-associated virus expressing Cre in an Flp-dependent manner (AAV-FRT-stop-FRT-Cre-GFP). This approach allowed restricted deletion of $ErbB4$ in the TRN area (Supplementary Fig. 5) and, remarkably, resulted in improved learning in the basic 2-AC task – a phenotype that resembles that of the $SOM^{ErbB4-/-}$ mice (Supplementary Fig. 2). Importantly, compared with controls, mice with $ErbB4$ deletion in the TRN had enhanced performance in the auditory/auditory task but decreased performance in the incongruent trials of the visual/auditory task (Fig. 3d–f), behavioral phenotypes that mimic those of the $SOM^{ErbB4+/-}$ or $SOM^{ErbB4-/-}$ mice. These results indicate that the observed behavioral alterations in the $SOM^{ErbB4+/-}$ or $SOM^{ErbB4-/-}$ mice are caused by ErbB4 deficiency in TRN.

ErbB4 suppresses cortical drive onto the TRN

Since ErbB4 modulates synapse development and function in a number of brain areas and cell types^{18,19,32–36}, we next investigated the effects of ErbB4 deficiency on excitatory synaptic transmission onto TRN neurons. We recorded pairs of adjacent SOM^+ (red-fluorescent) and SOM^- (non-fluorescent) TRN neurons in acute brain slices (Fig. 1a; Fig. 4a). Excitatory postsynaptic currents (EPSCs) were evoked by a stimulating electrode placed at the border between TRN and the internal capsule. In WT mice, EPSCs recorded from SOM^+ cells were significantly smaller than those from SOM^- neurons (Fig. 4b), indicating that the strength of excitatory synapses onto SOM^+ neurons is weaker than that onto SOM^- neurons. Surprisingly, in the $SOM^{ErbB4+/-}$ (HET) or $SOM^{ErbB4-/-}$ (KO) mice, synaptic strength onto SOM^+ TRN neurons was markedly enhanced, such that EPSCs mediated by both AMPA receptors (AMPA) and NMDA receptors (NMDA) were much larger in SOM^+ neurons than in SOM^- neurons (Fig. 4b). These results indicate that ErbB4 signaling normally dampens the excitatory synapses onto SOM^+ TRN neurons, in contrast to what is seen in other brain areas, where ErbB4 most often acts to strengthen synapses^{18,19,32–36}.

Excitatory inputs to the TRN originate either from the corticothalamic (CT) projections that impart “top-down” control, or from the thalamocortical (TC) projections that convey “bottom-up” sensory information¹. The methods used in the above experiments could not distinguish between these projections. To determine which input is strengthened by ErbB4 deficiency, we injected the cortex or thalamus with an AAV-CAG-ChR2(H134R)-YFP to express the light-sensitive cation channel channelrhodopsin-2 (ChR2)³⁷ in neurons that give rise to either the CT or TC projections (Fig. 5a, b; Supplementary Fig. 6). We next used a minimal photo-stimulation protocol, which permits measurement of the strength of single synapses¹⁷, to stimulate each pathway in acute slices while recording the ‘evoked minimal’

EPSCs (emEPSCs) in SOM⁺ TRN neurons. The emEPSCs driven by the CT projections, including those originating from the somatosensory, visual, and auditory cortices, were much larger in the ErbB4 mutant mice than in the WT littermates (Fig. 5c, d; Supplementary Fig. 6). In contrast, emEPSCs driven by the TC pathway were similar across different genotypes (Fig. 5c, d). These results indicate that deficient ErbB4 expression in SOM⁺ TRN neurons causes selective strengthening of the excitatory synapses driven by cortical inputs.

ErbB4 controls cortical modulation of thalamus via the TRN

It is possible that the increased cortical drive onto SOM⁺ TRN neurons leads to enhanced cortical feedback modulation of thalamic function, because activation of TRN neurons has been shown to potently modulate the activity of thalamic relay neurons^{6,38}. To test this hypothesis, we optogenetically stimulated the CT pathway and recorded the evoked synaptic responses in thalamic neurons (Fig. 5e, f). In each neuron we recorded both the monosynaptic EPSCs and the disynaptic IPSCs (inhibitory postsynaptic currents)³⁹ in response to the same photo-stimulation (Fig. 5e, f; Supplementary Fig. 7). We found that the IPSC to EPSC ratio in thalamic neurons was drastically increased by ErbB4 deficiency, and the effect was stronger in the KO than HET mice (Fig. 5f). This increased IPSC to EPSC ratio could be the result of either potentiated input onto SOM⁺ TRN neurons or enhanced output from these neurons, as ErbB4 has been shown to modulate presynaptic GABA release^{16,40}. However, deletion of ErbB4 did not change the paired-pulse ratio – an indicator of presynaptic release probability – of IPSCs onto thalamic neurons that were driven by SOM⁺ TRN neurons (Fig. 6). Thus, these results indicate that ErbB4 deficiency in SOM⁺ TRN neurons enhances the TRN-mediated modulation of thalamic neurons, an effect that can be explained at least in part by increased cortical drive.

ErbB4 regulates sensory selection via cortico-TRN circuit

One possible cause of the behavioral phenotypes in the ErbB4 mutant mice is the potentiation of synapses onto SOM⁺ TRN neurons driven by the CT inputs (Fig. 5, Supplementary Fig. 6). To test this possibility, we sought to reverse this enhanced cortical drive in the KO mice. As excitatory synaptic transmission onto TRN neurons driven by cortical inputs is mediated by GluA4-containing AMPARs¹⁷, we exploited the C-terminal tail of GluA4 (GluA4-C-tail), which blocks GluA4 trafficking thereby depressing synaptic transmission⁴¹. We bilaterally injected the TRN of the KO (*SOM⁺ErbB4^{-/-}*) mice with an AAV-DIO-GluA4-C-tail-GFP that harbors a double floxed inverted open reading frame (DIO), which expresses the GluA4-C-tail tagged with GFP in a Cre-dependent manner (Supplementary Fig. 8 a–c).

Expression of GluA4-C-tail in SOM⁺ TRN neurons in the KO mice selectively weakened the excitatory synaptic transmission driven by the CT inputs (Fig. 7a, b), without affecting that driven by the TC inputs (Fig. 7c, d). This result is consistent with previous finding that deletion of GluA4 depresses synaptic transmission onto TRN neurons driven by the CT pathway, but not that driven by the TC pathway¹⁷. In subsequent behavioral experiments we found that expression of GluA4-C-tail in SOM⁺ TRN neurons reduced the speed of learning of KO mice in the basic 2-AC tasks, to a level that is comparable to that of WT (Supplementary Fig. 9a, b). Remarkably, the same manipulation decreased the performance

of KO mice in the auditory/auditory task while enhancing their performance in the incongruent trials of the visual/auditory task. As a result, these mice performed similarly to WT mice in both tasks (Fig. 8a, b). The behavioral effect of GluA4-C-tail was dependent on the efficiency of viral infection in TRN (Supplementary Fig. 8c), demonstrating the specificity and potency of this manipulation. In addition, expression of GluA4-C-tail in SOM⁺ TRN neurons did not affect performance in the congruent trials of the visual/auditory task (Fig. 8c), nor did it affect performance in a sensory perception test (Supplementary Fig. 9c–e).

Thus, reversal of the enhanced cortical drive by selective expression of GluA4-C-tail in SOM⁺ TRN neurons was sufficient to “rescue” the behavioral phenotypes of the ErbB4 mutant mice, normalizing both the enhanced performance in the within-modality task and the impaired performance in the across-modalities task.

DISCUSSION

Previous studies aimed at determining the causal relationship between TRN function and behavior have relied on lesions of TRN, which in general cause attention-related behavioral deficits^{11,42}. However, because of the thin and elongated shape of TRN and its close proximity to the dorsal thalamus, off-target effects in lesion studies are almost unavoidable and can confound the explanation of results. With the advent of new technologies, in particular mouse genetic and optogenetic techniques that allow selectively targeting of TRN neurons, recent studies have made important progress in understanding the role of TRN in sleep/wakefulness transitions and in broad shifts in arousal state^{5,38}.

Another important role that has been attributed to TRN is its participation in goal-directed attention^{3,8,9}, a fundamental cognitive function whereby behaviorally relevant sensory information is selected against irrelevant sensory information for further processing and for guiding goal-directed behavior^{31,43}. Goal-directed attention extensively interacts with perception, working memory, learning, and executive control¹⁵; therefore, it is difficult to distinguish altered attention from changes in these other cognitive functions in behavioral assays. Previous studies on the role of TRN in goal-directed attention were mainly carried out in monkeys, a species that is versatile in complex tasks designed to assess attention in isolation^{8,9}. However, monkeys are impervious to molecular and neural circuit manipulations that are required for understanding the mechanisms of TRN function.

We overcame these challenges by devising behavioral tasks that engage goal-directed attention in mice, and by selectively targeting and manipulating the cortico-TRN-thalamic circuit. This approach allowed us to uncover an important role of ErbB4 in shaping cortical feedback control of TRN function, and in regulating performance in tasks demanding attention. Specifically, we show that ErbB4 deficiency in SOM⁺ TRN neurons markedly altered the performance of mice in sensory selection tasks, consistent with changes in goal-directed attention. Furthermore, ErbB4 deficiency selectively potentiates the excitatory synapses onto SOM⁺ TRN neurons driven by cortical inputs, thereby enhancing the TRN-mediated cortical feedback modulation of thalamic neurons. Finally, by adjusting the strength of the cortico-TRN synapses, we were able to rescue the ErbB4 deficiency-induced

changes in behavioral performance. The most parsimonious explanation for these results is that TRN circuit dysfunction driven by the enhanced cortical excitatory inputs is the major cause of the observed behavioral phenotypes.

The majority of TRN neurons do not form reciprocal connections with thalamic neurons; instead, they form “open-loop” connections with thalamic neurons^{1,20,44} (see a model diagram in Supplementary Fig. 10). These open loops provide anatomical basis for lateral inhibition in the thalamus, which can suppress thalamic responses to distractors while allowing responses to the attended stimuli (the “targets”) to reach cortex^{1,9,20,44} (Supplementary Fig. 10a). This lateral inhibition is presumably enhanced in the ErbB4 mutant mice as a result of the enhancement in cortical drive, leading to increased signal-to-noise ratio in the thalamus, and thus improved performance in the auditory/auditory and visual/visual tasks (Fig. 3a; Supplementary Fig. 4a, b).

Why, then, did the ErbB4 mutant mice display impaired performance in the across-modalities tasks (Fig. 3b; Supplementary Fig. 4c, d)? Unlike the within-modality task, in an across-modalities task the mice need to globally switch attention across modalities. It is known that attending to an auditory stimulus suppresses neuronal activity in the visual TRN^{8,9}, an effect that could be mediated by the reticulo-reticular inhibition^{45,46}. In addition, cross modality interactions may also occur through TRN-mediated inhibition across different thalamic nuclei^{47–49} (see Supplementary Fig. 10b). It is possible that, in order to select the relevant stimuli and make correct choices in our across-modalities tasks, it is necessary for neurons in the relevant TRN sector to be activated and those in the irrelevant sector inhibited (Supplementary Fig. 10b). This will lead to disinhibition and inhibition, respectively, of the corresponding thalamic areas and allow the relevant stimuli to reach the cortex (Supplementary Fig. 10b). Furthermore, one challenge of these tasks – as is already alluded to in a previous section – lies in the fact that even the irrelevant cues are capable of engaging in goal-directed (top-down) attention thereby affecting performance, because these cues are initially used to guide behavior during training (Supplementary Fig. 10b, indicated by arrows from the cortex; also see Methods). This problem is worsened in the ErbB4 mutant mice, in which the aberrantly enhanced excitatory cortical inputs onto SOM⁺ TRN neurons increase the sensitivity of these neurons to top-down signals and therefore their likelihood to escape inhibition, leading to decreased signal-to-noise ratio in the TRN and an apparent behavioral perseverance to the irrelevant cues (Supplementary Fig. 10b).

Together, our results indicate that the SOM⁺ TRN neurons have an important role in selecting targets from distractors, and in preferentially processing behaviorally relevant sensory inputs in situations where competing sensory stimuli direct conflicting actions. Our results also suggest that normal levels of ErbB4, by regulating cortical excitatory synaptic transmission onto SOM⁺ TRN neurons, tunes the function of the cortico–TRN–thalamic circuit, allowing a balance between the ability to attend to selective sensory inputs and the flexibility of refocusing attention according to behavioral needs.

Our study reveals a novel synaptic function of ErbB4 in the TRN that is distinct from the reported actions of this signaling molecule in other CNS regions¹⁸, and sheds light on a mechanistic link between ErbB4 genetic defects, TRN circuit dysfunction, and abnormalities

in goal-directed attention. This is particularly interesting considering that both defects in NRG1/ErbB4 signaling and dysfunction of TRN circuitry have been implicated in schizophrenia^{2,18}, and that impairments in goal-directed attention are thought to underlie major cognitive symptoms of the disease¹⁵.

METHODS

A Supplementary Methods Checklist is available.

Animals

Mice were housed in a temperature- and humidity-controlled environment with a 12-h light-dark cycle (9 a.m. to 9 p.m. light) in groups of 2–5 animals. All behavioral experiments were performed in the light cycle. Mice used in all behavior experiments had free access to food, but water was restricted to behavioral sessions. Free water was provided on days with no experimental sessions. For mice used in other experiments, food and water were freely available. Both male and female mice were used in all experiments, and the data was pooled as no gender difference was observed. The *Som-Cre*²³, *Som-Flp*⁵⁰, *H2b-GFP*¹⁴, and *ErbB4^{lox/lox}*²⁸ mice were generated as described. The *Ai14* reporter mice²⁴ were purchased from The Jackson Laboratory. All mice have been bred onto C57BL/6N background for at least 5 generations. Mice of 2–4 months of age were used for all the behavioral experiments. All procedures involving animals were approved by the Institute Animal Care and Use Committees of Cold Spring Harbor Laboratory and carried out in accordance with National Institutes of Health standards.

Viral vectors

All AAV viruses, such as the AAV-CAG-ChR2(H134R)-YFP, AAV-DIO-ChR2(H134R)-YFP, AAV-DIO-GluA4-C-tail, AAV-DIO-GFP, AAV-FRT-stop-FRT-Cre-GFP, and AAV-FRT-stop-FRT-GFP were produced by the University of North Carolina Vector Core Facilities. All viral vectors were stored in aliquots at –80 °C until use.

Immunohistochemistry

Immunohistochemistry experiments were performed following standard procedures. Briefly, mice were anesthetized and perfused with PBS, followed by perfusion with 4% paraformaldehyde (PFA). Brains were extracted and further fixed in 4% PFA overnight at 4 °C followed by cryoprotection in a 30% PBS-buffered sucrose solution for 36 h. Coronal sections (40–50 µm) were cut using a freezing microtome (Leica SM 2010R, Leica). Sections were first washed in PBS (3 × 5 min) and then incubated in PBST (0.3% Triton X-100 in PBS) for 30 min at room temperature (RT), followed by washing with PBS (3 × 5 min). Next, sections were blocked in 5% normal goat serum in PBST for 30 min at RT, followed by incubation with primary antibodies overnight at 4 °C. Sections were then washed with PBS (5 × 15 min) and incubated with fluorescent secondary antibodies at RT for 1 h. After washing with PBS (5 × 15 min), sections were mounted onto slides with Fluoromount-G (Beckman Coulter). Images were taken using a LSM 710 laser-scanning confocal microscope (Carl Zeiss). The primary antibodies used were: anti-ErbB4 (mouse,

Fisher Scientific, MS 270P, 1:200), anti-somatostatin (rabbit, Bachem, T 4103, 1:2000), and anti-NeuN (mouse, Millipore, MAB377, 1:100).

Behavioral tasks

Basic two-alternative choice tasks: both an auditory and a visual two-alternative choice (2-AC)^{29,30} procedure were used (see Fig. 2a, b). Mice initiated each trial by poking their nose into the center port of a three-port operant chamber. After a silent delay of random duration (200–300 ms, uniformly distributed), a frequency-modulated target sound, or a light stimulus, was presented. In the auditory task, the carrier frequency of the target indicated to the animal which of the two side ports would provide 10 μ l of water reward. For a target carrier frequency of 8 kHz, reward was available only at the left port. For a target of 20 kHz, reward was provided at the right port. Mice were only rewarded in trials in which they chose the correct port as their first choice. Sound intensity was set at 60 dB-SPL, and sound duration was 100 ms. The modulation frequency was set to 15 Hz. In the visual task, a light signal of 500 ms duration from the left port indicated reward on the left side, and a light signal from the right port was rewarded on the right side. Mice were required to stay in the center port until the target was presented. If the animal withdrew before the onset of the target, the trial was considered invalid and was aborted. A new trial would then be initiated. Behavioral analysis included only valid trials in which the animal stayed in the center port until the time of target onset. In both the auditory and visual 2-AC, incorrect choices were punished by a 4 s timeout and a white noise.

Auditory/auditory task: as in the basic auditory 2-AC task, mice initiated a trial by a nose poke into the center port. After a silent delay of 50 ms, a train of five 100-ms pure tone distractors was presented (Fig. 2c). The frequency of each of the five distractor tones in the train was 5, 8, 12.5, 16 and 20 kHz, and the order in which the tones were presented was random for each trial. In each trial, one target (the 8 kHz or 20 kHz frequency-modulated sound in the basic 2-AC tasks described above) was embedded in the train of distractors. It should be noted that the frequency-modulated 20 kHz sound has distinct physical properties compared with the 20 kHz pure tone. The position of the target in a train was randomized between 100 and 300 ms after the onset of the first distractor tone (Fig. 2c). The performance of each mouse was monitored over three sessions.

Visual/auditory task: in this task, the light and sound stimuli were presented simultaneously, and the animal was only rewarded for correct responses to the light stimuli (Fig. 2d). Trials in which the two stimuli are congruent or incongruent were chosen randomly. The performance of each mouse was monitored over five sessions.

Visual/visual task: an LED array (3.4 cm \times 3.4 cm, Linksprite) consisting of 8 \times 8 single red LEDs was mounted above the left and right side port (Supplementary Fig. 4a). The target visual cues were continuous illumination (500 ms, indicated in red) of four LEDs in the center of the left and right arrays, signaling reward on the left and right, respectively. Mice were first trained to respond to those target cues until reaching performance criteria (above 75% correct trials for three consecutive sessions), and subsequently tested in sessions in which distractor lights were added. The distractors were lights flashing (at 20 Hz) simultaneously from both LED arrays, and were generated by two random LEDs

surrounding the four center LEDs in each array. Target cues and distractor lights started 100 ms after the animal initiated the trial by nose poking into the center port. The targets stayed on for 500 ms, whereas the distractors were terminated after 400 ms.

Auditory/visual task: same as the visual/auditory task, except that the relevant and irrelevant cues were swapped (Supplementary Fig. 4c).

Auditory discrimination task—Mice used in this experiment were first trained in the basic auditory 2-AC task to reach performance criteria. Mice initiated a trial by a nose poke into the center port. After a silent delay of random duration (200–300 ms), a frequency modulated target sound was presented for 100 ms. The frequency of the sound was randomly selected from a group of eight frequencies (8, 9.119, 10.39, 11.85, 13.5, 15.39, 17.55, and 20 kHz). These frequencies were chosen such that they were equidistant from each other on the logarithmic scale (Supplementary Fig. 3a–c & 9c–e). All frequencies less than 12.65 KHz (the geometric mean of 8 and 20 KHz) were rewarded if the mouse chose the left water port, and those greater than 12.65 kHz were rewarded with water in the right water port. The volume of the water reward was decreased to 5 μ l to ensure that the mice performed sufficient number of trials for each of the frequencies. Data from five consecutive sessions were collected (250–350 trials per session).

Data analysis: the response of a mouse to each of the eight sound frequencies was transformed into the percentage of ‘rightward selection’, which is the percentage of the trials in which the mouse chose the water port on the right side (Supplementary Fig. 3 & 9). This data was fitted using the following logistic function⁵¹:

$$y = \frac{A1 - A2}{1 + (X_0/X)^p} + A2$$

where X_0 represents the median threshold and p determines the slope of the curve; $A1$ and $A2$ are the upper and lower bounds of the equation, respectively. A sigmoidal psychometric curve was thus generated. The median threshold X_0 and parameter p of this curve were then obtained for each animal, and the data was pooled for each group.

Visual discrimination task—A horizontal panel (8 cm \times 0.9 cm, Kingbright) with eight individually illuminable LEDs was mounted above the water ports (Supplementary Fig. 3d). Four LEDs were evenly distributed on either side of the midline of the center port. The center-to-center distance between adjacent LEDs was 1 cm, such that the illumination center of the individual LEDs was positioned at 0.5, 1.5, 2.5 and 3.5 cm from the midline of the center port. Mice were first trained to criteria in the basic visual 2-AC task, in which illumination of LEDs in the leftmost and rightmost indicated reward on the left and right, respectively. They were then tested for discrimination of illumination at the eight positions. In each trial, one of the eight LEDs was illuminated for 300 ms. As in the auditory discrimination task, the volume of the water reward was decreased to 5 μ l and data from five consecutive sessions were collected. Data analysis was carried out in the same way as that described for the auditory discrimination task.

Order of animal training and testing—For animals used in the auditory/auditory, visual/auditory or auditory/visual task:

1. Training in the auditory basic 2-AC task until performance has reached criteria (>75% in three consecutive sessions);
2. Testing in the auditory/auditory task for three sessions;
3. Training in the visual basic 2-AC task until performance has reached criteria (>75% in three consecutive sessions);
4. Repeat the auditory basic 2-AC task (step #1) for one or two sessions. This is to make sure that performance in this task has not been affected by the other tasks;
5. Testing in the visual/auditory or auditory/visual task for five sessions. Note that different groups of mice were used for the visual/auditory or auditory/visual task, as these tasks may influence each other.

For animals used in the visual/visual and visual discrimination task:

1. Training in the visual basic 2-AC task until performance has reached criteria (>75% in three consecutive sessions);
2. Testing in the visual discrimination task for five sessions;
3. Training mice to respond to the target stimuli of the visual/visual task until performance has reached criteria;
4. Testing in the visual/visual task for three sessions

During the training phase animals were trained for two 30 – 45 min sessions per day. In testing phase, each session was 30 min, and one session was given in each experimental day for all animals. Each animal performed on average about 200 – 250 valid trials per session. There were three possible behavioral outcomes: correct response, incorrect response, and omission. Trials in which animal failed to make any response within 4 sec after target presentation were counted as omissions, which were usually rare (< 5% of all valid trials). Performance was calculated as the percentage of correct responses in all valid trials.

Stimulus delivery: auditory stimuli were delivered through generic electromagnetic dynamic speakers calibrated using a pressure-field microphone (Brüel & Kjær) to produce 60 dB-SPL in the range of 5–40 kHz at the position of the subject. Waveforms were created in software at a sampling rate of 200,000 samples per second and delivered to speakers through a *Lynx L22* sound card (Lynx Studio Technology). We applied rise and fall linear envelopes of 2 ms to all sounds.

Stereotaxic surgery

Standard surgical procedures were followed for stereotaxic injection⁵². Briefly, mice were anesthetized with ketamine (100 mg/kg) supplemented with xylazine (10 mg/kg) and positioned in a stereotaxic injection frame (myNeuroLab.com). A digital mouse brain atlas was linked to the injection frame to guide the identification and targeting of different brain areas (Angle Two Stereotaxic System, myNeuroLab.com). Viruses were delivered with a

glass micropipette through a skull window (1–2 mm²) by pressure application (5–12 psi, controlled by a Picospritzer III, General Valve, Fairfield, NJ, USA). The injections were performed using the following stereotaxic coordinates for TRN: –0.82/–1.34/–1.82 mm from Bregma, 1.9/2.4/2.4 mm lateral from the midline, and 3.8 to 3.2 mm vertical from the cortical surface; for thalamus: –1.70 mm from Bregma, 1.45 mm lateral from the midline, and 3.5 mm vertical from the cortical surface; for somatosensory cortex: –0.82 mm from Bregma, 2.7 mm lateral from the midline, and 2.05 mm vertical from the cortical surface; for auditory cortex: –2.80 mm from Bregma, 3.88 mm lateral from the midline, and 2.70 mm vertical from the cortical surface; for visual cortex: –3.28 mm from Bregma, 2.30 mm lateral from the midline, and 1.20 mm vertical from the cortical surface. During all surgical procedures, mice were kept on a heating pad and were brought back to their home cages after regaining movement. For postoperative care, mice were hydrated by intraperitoneal injection with 0.3–0.5 ml of lactated ringers. We used metacam (meloxicam, 1–2 mg/kg) as an analgesic and to reduce inflammation. We injected 1–1.5 µl of viral solution (~10¹² virus particles/ml) bilaterally into TRN, or 0.5 µl into the cortex or thalamus, and waited approximately 2–3 weeks to allow maximal viral expression. Note that multiple locations in the TRN were targeted to ensure sufficient infection by viruses.

Preparation of acute brain slices and electrophysiology

Mice of 16–25 days (for electrophysiological recordings in the TRN) or 6–8 weeks (for recordings in the thalamus) of age were used. Mice were anesthetized with isoflurane, decapitated, and their brains quickly removed and chilled in ice-cold dissection buffer (110.0 mM choline chloride, 25.0 mM NaHCO₃, 1.25 mM NaH₂PO₄, 2.5 mM KCl, 0.5 mM CaCl₂, 7.0 mM MgCl₂, 25.0 mM glucose, 11.6 mM ascorbic acid and 3.1 mM pyruvic acid, gassed with 95% O₂ and 5% CO₂). Horizontal slices (300 µm) containing the TRN were cut in the dissection buffer using a HM650 Vibrating Microtome (MICROM International GmbH, Walldorf, Germany), and subsequently transferred to a storage chamber containing artificial cerebrospinal fluid (ACSF) (118 mM NaCl, 2.5 mM KCl, 26.2 mM NaHCO₃, 1 mM NaH₂PO₄, 20 mM glucose, 1 mM MgCl₂ and 2 mM CaCl₂, at 34 °C, pH 7.4, gassed with 95% O₂ and 5% CO₂). After at least 40 min recovery time, slices were transferred to room temperature and were constantly perfused with ACSF.

In acute slices the TRN can be easily identified under trans-illumination. In addition, we took advantage of the *Som-Cre;Ai14* line, in which the TRN had very high density of SOM⁺ neurons that are red fluorescent (Fig. 1a), to facilitate the identification of TRN under epifluorescence illumination.

Simultaneous whole-cell patch-clamp recordings from SOM⁺/SOM[–] neuronal pairs in TRN were obtained with Multiclamp 700B amplifiers (Molecular Devices, Sunnyvale, CA, USA). Recordings were performed under visual guidance using an Olympus BX51 microscope equipped with both transmitted light illumination and epifluorescence illumination. The SOM⁺ cells were identified based on their red-fluorescence from tdTomato. For evoked EPSCs, synaptic responses were evoked with a bipolar stimulating electrode placed in the border between the TRN and internal capsule, approximately 0.2 mm away from the recorded cell bodies in TRN. Electrical stimulation was delivered every 30 seconds and

synaptic responses were low-pass filtered at 1 KHz and recorded at holding potentials of -70 mV (for AMPAR-mediated responses), $+40$ mV (for NMDAR-mediated responses), or 0 mV (for GABA-A-receptor-mediated responses). NMDAR-mediated responses were quantified as the mean current between 50 ms and 100 ms after stimulation. Recordings were performed in the ACSF. The internal solution for voltage-clamp experiments contained 115 mM cesium methanesulphonate, 20 mM CsCl, 10 mM HEPES, 2.5 mM $MgCl_2$, 4 mM Na_2 -ATP, 0.4 mM Na_3 GTP, 10 mM Na-phosphocreatine and 0.6 mM EGTA (pH 7.2). Evoked EPSCs in certain experiments were recorded with picrotoxin ($100 \mu M$) added to the ACSF as indicated. Electrophysiological data were acquired and analyzed using pCLAMP 10 software (Molecular Devices).

To evoke synaptic transmission using the optogenetic methods, the AAV-CAG-ChR2(H134R)-YFP or AAV-DIO-ChR2(H134R)-YFP was injected into different brain regions, including cortex, thalamus, and TRN, and allowed to express for 10–14 days. Acute brain slices were prepared and a blue light was used to stimulate ChR2. The light source was a single-wavelength LED system ($\lambda = 470$ nm; CoolLED.com) connected to the epifluorescence port of an Olympus BX51 microscope. Light pulses of 0.2–0.5 ms, triggered by a TTL signal from the Clampex software (Molecular Devices), were used to evoke synaptic transmission. We used a minimal photo-stimulation protocol as previously described¹⁷, in which the photo-stimulation resulted in 50–70% failures and low response-amplitude variability of the ‘evoked minimal’ EPSCs (emEPSCs). The emEPSCs presumably represent responses of single synapses driven by the CT or TC pathway¹⁷.

Statistics and data presentation

Data were analyzed with GraphPad Prism Software. The sample size was estimated using power analysis based on our preliminary studies. Normality was tested by D’Agostino-Pearson or Shapiro-Wilk normality test. Statistical analysis was performed using paired or unpaired two-tailed Student’s *t*-test, and one-way ANOVA or two-way ANOVA as indicated, followed by Tukey’s or Bonferroni’s *post hoc* test to correct for multiple comparisons. $P < 0.05$ was considered significant. No randomization was used to assign experimental groups, but mice were assigned to specific experimental groups without bias. Behavioral tests and electrophysiological data acquisition were performed by an investigator with knowledge of the identity of the experimental groups. All behavior experiments were controlled by computer systems, and data were collected and analyzed in an automated and unbiased way. No single data points were excluded. Animals that did not learn the basic 2-AC task within 35 sessions were excluded. Virus-injected animals in which the injection site was incorrect were excluded.

Supplementary Material

Refer to Web version on PubMed Central for supplementary material.

Acknowledgments

We thank A. Zador for help on the behavioral paradigms, J.J. Zhu for the GluA4-C-tail construct, and A. Churchland for advice on the visual/visual task. We thank F. Albeanu, A. Kepecs, H. Kessels, R. Malinow, L. Mei, S. Shea, P. Smith, and L. Van Aelst for critical reading of earlier versions of the manuscript, and members of the Li

Lab for discussions. This study was supported by a fellowship from DFG (S.A.), and grants from NIH (B.L. and Z.J.H.), the Dana Foundation (B.L.), NARSAD (S.A., B.L., and Z.J.H.), Louis Feil Trust (B.L.), and Stanley Family Foundation (B.L. and Z.J.H.).

References

1. Zikopoulos B, Barbas H. Circuits formultisensory integration and attentional modulation through the prefrontal cortex and the thalamic reticular nucleus in primates. *Rev Neurosci.* 2007; 18:417–438. [PubMed: 18330211]
2. Ferrarelli F, Tononi G. The thalamic reticular nucleus and schizophrenia. *Schizophr Bull.* 2010; 37:306–315. [PubMed: 21131368]
3. Crick F. Function of the thalamic reticular complex: the searchlight hypothesis. *Proc Natl Acad Sci U S A.* 1984; 81:4586–4590. [PubMed: 6589612]
4. Pinault D. The thalamic reticular nucleus: structure, function and concept. *Brain Res Brain Res Rev.* 2004; 46:1–31. [PubMed: 15297152]
5. Halassa MM, et al. State-dependent architecture of thalamic reticular subnetworks. *Cell.* 2014; 158:808–821. [PubMed: 25126786]
6. Yu XJ, Xu XX, He S, He J. Change detection by thalamic reticular neurons. *Nat Neurosci.* 2009; 12:1165–1170. [PubMed: 19684591]
7. Krause M, Hoffmann WE, Hajos M. Auditory sensory gating in hippocampus and reticular thalamic neurons in anesthetized rats. *Biological psychiatry.* 2003; 53:244–253. [PubMed: 12559658]
8. McAlonan K, Cavanaugh J, Wurtz RH. Guarding the gateway to cortex with attention in visual thalamus. *Nature.* 2008; 456:391–394. [PubMed: 18849967]
9. McAlonan K, Cavanaugh J, Wurtz RH. Attentional modulation of thalamic reticular neurons. *J Neurosci.* 2006; 26:4444–4450. [PubMed: 16624964]
10. McAlonan K, Brown VJ, Bowman EM. Thalamic reticular nucleus activation reflects attentional gating during classical conditioning. *J Neurosci.* 2000; 20:8897–8901. [PubMed: 11102499]
11. Weese GD, Phillips JM, Brown VJ. Attentional orienting is impaired by unilateral lesions of the thalamic reticular nucleus in the rat. *J Neurosci.* 1999; 19:10135–10139. [PubMed: 10559421]
12. Pinault D. Dysfunctional thalamus-related networks in schizophrenia. *Schizophrenia bulletin.* 2011; 37:238–243. [PubMed: 21307040]
13. Zhang Y, Llinas RR, Lisman JE. Inhibition of NMDARs in the Nucleus Reticularis of the Thalamus Produces Delta Frequency Bursting. *Front Neural Circuits.* 2009; 3:20. [PubMed: 20057928]
14. Schulman JJ, et al. Imaging of thalamocortical dysrhythmia in neuropsychiatry. *Front Hum Neurosci.* 2011; 5:69. [PubMed: 21863138]
15. Luck SJ, Gold JM. The construct of attention in schizophrenia. *Biol Psychiatry.* 2008; 64:34–39. [PubMed: 18374901]
16. Woo RS, et al. Neuregulin-1 Enhances Depolarization-Induced GABA Release. *Neuron.* 2007; 54:599–610. [PubMed: 17521572]
17. Paz JT, et al. A new mode of corticothalamic transmission revealed in the Gria4(-/-) model of absence epilepsy. *Nature neuroscience.* 2011; 14:1167–1173. [PubMed: 21857658]
18. Mei L, Xiong WC. Neuregulin 1 in neural development, synaptic plasticity and schizophrenia. *Nat Rev Neurosci.* 2008; 9:437–452. [PubMed: 18478032]
19. Mei L, Nave KA. Neuregulin-ERBB signaling in the nervous system and neuropsychiatric diseases. *Neuron.* 2014; 83:27–49. [PubMed: 24991953]
20. Zikopoulos B, Barbas H. Pathways for emotions and attention converge on the thalamic reticular nucleus in primates. *The Journal of neuroscience: the official journal of the Society for Neuroscience.* 2012; 32:5338–5350. [PubMed: 22496579]
21. Clemence AE, Mitrofanis J. Cytoarchitectonic heterogeneities in the thalamic reticular nucleus of cats and ferrets. *The Journal of comparative neurology.* 1992; 322:167–180. [PubMed: 1381730]
22. Bouras C, Magistretti PJ, Morrison JH, Constantinidis J. An immunohistochemical study of pro-somatostatin-derived peptides in the human brain. *Neuroscience.* 1987; 22:781–800. [PubMed: 2891078]

23. Taniguchi H, et al. A resource of Cre driver lines for genetic targeting of GABAergic neurons in cerebral cortex. *Neuron*. 2011; 71:995–1013. [PubMed: 21943598]
24. Madisen L, et al. A robust and high-throughput Cre reporting and characterization system for the whole mouse brain. *Nat Neurosci*. 2010; 13:133–140. [PubMed: 20023653]
25. Neddens J, Buonanno A. Expression of the neuregulin receptor ErbB4 in the brain of the rhesus monkey (*Macaca mulatta*). *PLoS One*. 2011; 6:e27337. [PubMed: 22087295]
26. Yau HJ, Wang HF, Lai C, Liu FC. Neural development of the neuregulin receptor ErbB4 in the cerebral cortex and the hippocampus: preferential expression by interneurons tangentially migrating from the ganglionic eminences. *Cereb Cortex*. 2003; 13:252–264. [PubMed: 12571115]
27. Neddens J, Buonanno A. Selective populations of hippocampal interneurons express ErbB4 and their number and distribution is altered in ErbB4 knockout mice. *Hippocampus*. 2010; 20:724–744. [PubMed: 19655320]
28. Golub MS, Germann SL, Lloyd KC. Behavioral characteristics of a nervous system-specific erbB4 knock-out mouse. *Behav Brain Res*. 2004; 153:159–170. [PubMed: 15219717]
29. Uchida N, Mainen ZF. Speed and accuracy of olfactory discrimination in the rat. *Nature neuroscience*. 2003; 6:1224–1229. [PubMed: 14566341]
30. Jaramillo S, Zador AM. The auditory cortex mediates the perceptual effects of acoustic temporal expectation. *Nature neuroscience*. 2011; 14:246–251. [PubMed: 21170056]
31. Corbetta M, Shulman GL. Control of goal-directed and stimulus-driven attention in the brain. *Nat Rev Neurosci*. 2002; 3:201–215. [PubMed: 11994752]
32. Li B, Woo RS, Mei L, Malinow R. The Neuregulin-1 Receptor ErbB4 Controls Glutamatergic Synapse Maturation and Plasticity. *Neuron*. 2007; 54:583–597. [PubMed: 17521571]
33. Krivosheya D, et al. ErbB4-neuregulin signaling modulates synapse development and dendritic arborization through distinct mechanisms. *The Journal of biological chemistry*. 2008; 283:32944–32956. [PubMed: 18819924]
34. Fazzari P, et al. Control of cortical GABA circuitry development by *Nrg1* and ErbB4 signalling. *Nature*. 2010; 464:1376–1380. [PubMed: 20393464]
35. Ting AK, et al. Neuregulin 1 promotes excitatory synapse development and function in GABAergic interneurons. *The Journal of neuroscience: the official journal of the Society for Neuroscience*. 2011; 31:15–25. [PubMed: 21209185]
36. Cooper MA, Koleske AJ. Ablation of ErbB4 from excitatory neurons leads to reduced dendritic spine density in mouse prefrontal cortex. *The Journal of comparative neurology*. 2014; 522:3351–3362. [PubMed: 24752666]
37. Zhang F, Wang LP, Boyden ES, Deisseroth K. Channelrhodopsin-2 and optical control of excitable cells. *Nat Methods*. 2006; 3:785–792. [PubMed: 16990810]
38. Halassa MM, et al. Selective optical drive of thalamic reticular nucleus generates thalamic bursts and cortical spindles. *Nature neuroscience*. 2011; 14:1118–1120. [PubMed: 21785436]
39. Cruikshank SJ, Urabe H, Nurmikko AV, Connors BW. Pathway-specific feedforward circuits between thalamus and neocortex revealed by selective optical stimulation of axons. *Neuron*. 2010; 65:230–245. [PubMed: 20152129]
40. Chen YJ, et al. ErbB4 in parvalbumin-positive interneurons is critical for neuregulin 1 regulation of long-term potentiation. *Proceedings of the National Academy of Sciences of the United States of America*. 2010; 107:21818–21823. [PubMed: 21106764]
41. Zhu JJ, Esteban JA, Hayashi Y, Malinow R. Postnatal synaptic potentiation: delivery of GluR4-containing AMPA receptors by spontaneous activity. *Nature neuroscience*. 2000; 3:1098–1106. [PubMed: 11036266]
42. Bucherelli C, Tassoni G, Bures J. Differential effect of functional ablation of thalamic reticular nucleus on the acquisition of passive and active avoidance. *Int J Neurosci*. 1993; 73:77–84. [PubMed: 8132421]
43. Squire RF, Noudoost B, Schafer RJ, Moore T. Prefrontal contributions to visual selective attention. *Annual review of neuroscience*. 2013; 36:451–466.
44. Pinault D, Deschenes M. Anatomical evidence for a mechanism of lateral inhibition in the rat thalamus. *The European journal of neuroscience*. 1998; 10:3462–3469. [PubMed: 9824459]

45. Fuentealba P, Steriade M. The reticular nucleus revisited: intrinsic and network properties of a thalamic pacemaker. *Progress in neurobiology*. 2005; 75:125–141. [PubMed: 15784303]
46. Lam YW, Nelson CS, Sherman SM. Mapping of the functional interconnections between thalamic reticular neurons using photostimulation. *J Neurophysiol*. 2006; 96:2593–2600. [PubMed: 16855107]
47. Crabtree JW, Collingridge GL, Isaac JT. A new intrathalamic pathway linking modality-related nuclei in the dorsal thalamus. *Nature neuroscience*. 1998; 1:389–394. [PubMed: 10196529]
48. Crabtree JW, Isaac JT. New intrathalamic pathways allowing modality-related and cross-modality switching in the dorsal thalamus. *The Journal of neuroscience: the official journal of the Society for Neuroscience*. 2002; 22:8754–8761. [PubMed: 12351751]
49. Kimura A, Imbe H, Donishi T, Tamai Y. Axonal projections of single auditory neurons in the thalamic reticular nucleus: implications for tonotopy-related gating function and cross-modal modulation. *The European journal of neuroscience*. 2007; 26:3524–3535. [PubMed: 18052989]
50. Fenno LE, et al. Targeting cells with single vectors using multiple-feature Boolean logic. *Nature methods*. 2014; 11:763–772. [PubMed: 24908100]
51. Gilchrist JM, Jerwood D, Ismaiel HS. Comparing and unifying slope estimates across psychometric function models. *Percept Psychophys*. 2005; 67:1289–1303. [PubMed: 16502849]
52. Li H, et al. Experience-dependent modification of a central amygdala fear circuit. *Nature neuroscience*. 2013; 16:332–339. [PubMed: 23354330]

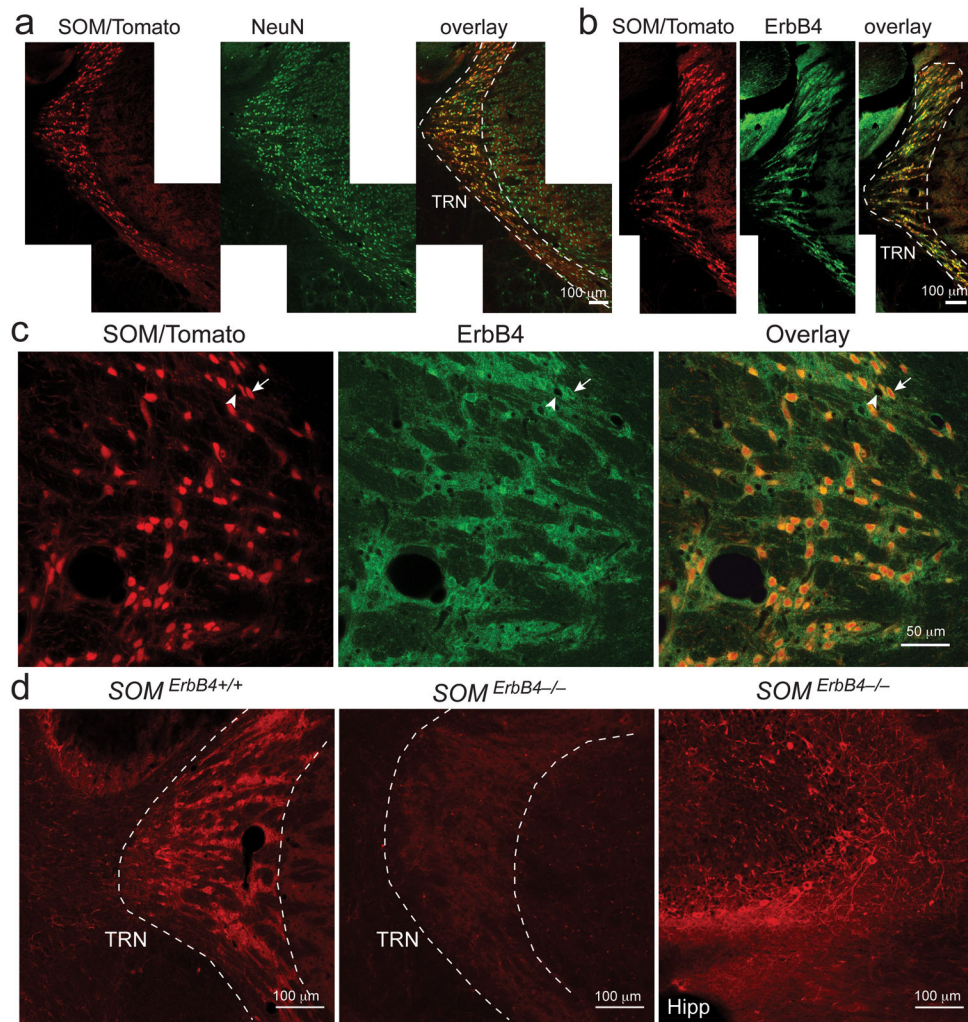


Figure 1. SOM^+ neurons are a major TRN population expressing ErbB4

(a) Left: a representative image of a coronal TRN section from a *Som-Cre;Ai14* mouse. SOM^+ neurons were identified on the basis of the intrinsic fluorescence of tdTomato (SOM/Tomato). Middle: the same brain section was processed for immunohistochemistry with an antibody recognizing NeuN to label all the neurons. Right: overlay; $79.89 \pm 2.37\%$ ($n = 2$ mice) of TRN neurons are SOM^+ . The border of TRN is outlined. (b) Representative images of TRN from a *Som-Cre;Ai14* mouse. Left: SOM^+ TRN neurons expressed tdTomato; middle: ErbB4 was recognized by an antibody. (c) High magnification images of neurons in the TRN, showing that tdTomato (red) and ErbB4 (green) are co-expressed in the same cells (overlay). Arrow denotes a SOM^+ neuron that had ErbB4 staining in the soma. Arrowhead denotes a SOM^- neuron that had no ErbB4 staining in the soma but was surrounded by fibers (presumably from other neurons) that had ErbB4 staining. $\sim 100\%$ of SOM^+ TRN neurons were recognized by the ErbB4 antibody ($n = 3$ mice). (d) Representative images of ErbB4 expression recognized by an antibody. Left and middle: ErbB4 was expressed in TRN neurons in a *SOM^{ErbB4}+/+* (WT) mouse (left), but not in a *SOM^{ErbB4}-/-* (KO) mouse (middle). Right: ErbB4 expression appeared normal in the hippocampus (Hipp) of the same KO mouse. Similar results were obtained in 3 WT and 3 KO mice.

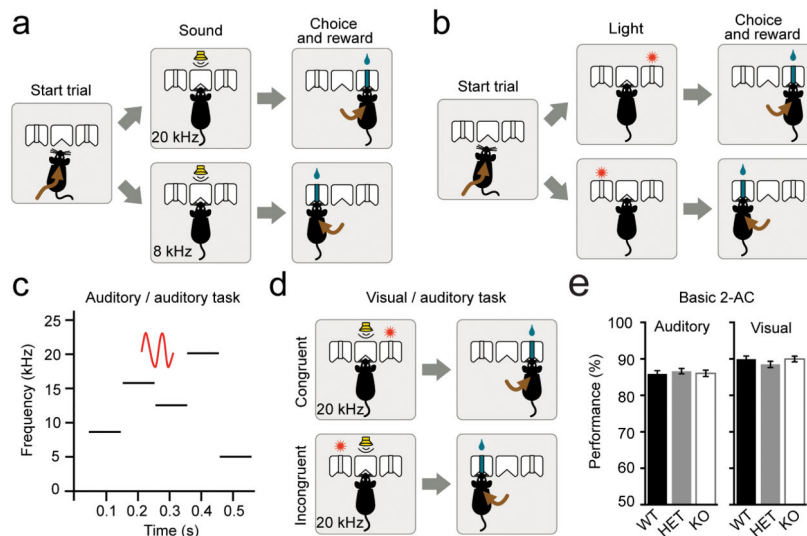


Figure 2. Behavioral tasks that assess sensory selection

(a & b), The basic 2-alternative choice (AC) tasks. (a) Auditory task: mice initiated each trial by a nose poke into the center port of the operant chamber. After a variable (200–300 ms) silent period, a frequency-modulated target sound was presented. Mice were required to stay in the port until the onset of the sound. The center frequency of the target sound (8 kHz or 20 kHz) indicated the side port where water reward would be delivered (left or right, respectively). Mice were only rewarded in trials in which they chose the correct port as their first response. (b) Visual task: same as in a, except that a nose poke into the center port turned on a light on the same side where water reward would be delivered (left or right). (c) After learning the basic auditory 2-AC task (see a), mice were tested in an “auditory/auditory” paradigm. As in the basic 2-AC task, mice initiated a trial by a nose poke into the center port. After a silent delay of 50 ms, a train of five 100-ms pure tone distractors was presented. The frequency of each of the five distractor tones in the train was 5, 8, 12.5, 16 and 20 kHz, and the order in which the tones were presented was random for each trial. In each trial, one of the frequency-modulated target sounds (denoted as a waveform in red), which indicated reward at one of the side ports (see a), was presented and immersed in the train of distractor tones (note that the frequency-modulated target sounds are qualitatively different from the pure tone distractors – see Methods). The position of the target in a train was randomized between 100 and 300 ms after the onset of the first distractor tone. Mice were required to stay in the port until the target was presented. (d) After learning both the auditory and the visual basic 2-AC tasks, mice were tested in a “visual/auditory” paradigm in which, after the nose poke into the center port, a light cue and one of the target sounds (8 kHz or 20 kHz) were simultaneously presented. However, only the light predicted reward, and the sound was random in relation to the reward. In order to obtain the reward, the mice had to attend to the light and ignore the sound. Congruent (top) and incongruent (bottom) trials occurred at the same frequency and were randomized. (e) The WT, HET, or KO mice had similar performance in the basic auditory (left) and visual (right) 2-AC tasks (auditory: WT, $85.87 \pm 0.88\%$, $n = 33$ mice, HET, $86.59 \pm 0.74\%$, $n = 28$ mice, KO, $86.03 \pm 0.85\%$, $n = 30$ mice, $F(2,88) = 0.20$, $P = 0.82$, one-way analysis of variance (ANOVA); visual: WT,

$89.9 \pm 0.87\%$, $n = 24$ mice, HET, $88.47 \pm 0.86\%$, $n = 22$ mice, KO, $89.95 \pm 0.79\%$, $n = 20$ mice, $F(2,63) = 0.97$, $P = 0.38$; one-way ANOVA). Data are presented as mean \pm s.e.m.

Author Manuscript

Author Manuscript

Author Manuscript

Author Manuscript

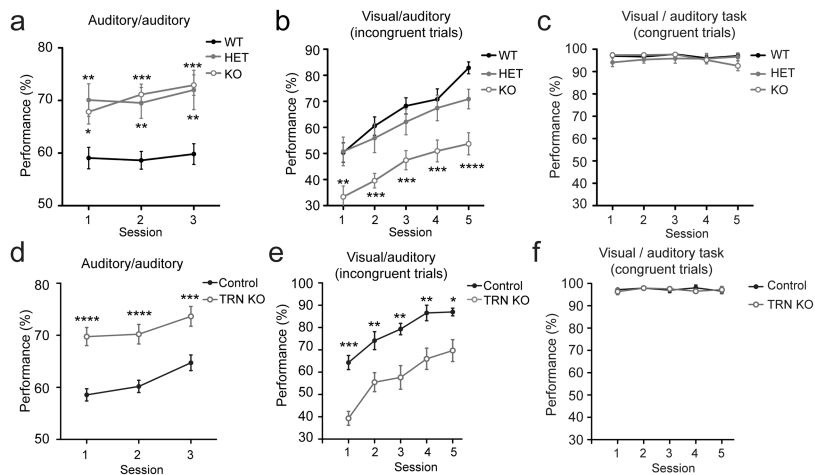


Figure 3. *ErbB4* deficiency in SOM^+ TRN neurons affects sensory selection

(a – c), behavioral phenotypes of WT, HET, and KO mice. (a) Reducing *ErbB4* levels in SOM^+ neurons improved performance in the auditory/auditory task (WT $n = 16$ mice, HET $n = 13$ mice, KO $n = 14$ mice; $F(2,40) = 11.06$; KO compared with WT: session 1, $*P = 0.025$, session 2, $***P = 0.0008$, session 3, $***P = 0.0006$; HET compared with WT: session 1, $**P = 0.0044$, session 2, $**P = 0.0048$, session 3, $**P = 0.0014$; Two-way repeated measures (RM) ANOVA followed by Tukey’s tests). (b & c) Reducing *ErbB4* levels in SOM^+ neurons impaired performance in the incongruent trials (b) (WT $n = 16$ mice, HET $n = 11$ mice, KO $n = 14$ mice; $F(2,38) = 11.38$; KO compared with WT: session 1, $**P = 0.005$, session 2, $***P = 0.0004$, session 3, $***P = 0.0004$, session 4, $***P = 0.0008$, session 5, $****P < 0.0001$; KO compared with HET: session 1, $P = 0.01$, session 2, $P = 0.017$, session 3, $P = 0.036$, session 4, $P = 0.016$, session 5, $P = 0.011$; Two-way RM ANOVA followed by Tukey’s tests), but not in the congruent trials (c) ($F(2,38) = 0.40$; $P = 0.67$, Two-way RM ANOVA), of the visual/auditory task. (d – f), behavioral phenotypes of mice in which *ErbB4* is selectively deleted in the TRN. “TRN KO”, *Som-Flp;ErbB4^{lox/lox}* mice in which the TRN was injected with a Flp-dependent AAV expressing Cre-GFP, so as to delete *ErbB4* in SOM^+ TRN neurons; “Control”, *Som-Flp;ErbB4^{lox/lox}* mice in which the TRN was injected with a Flp-dependent AAV expressing GFP. (d) Selective deletion of *ErbB4* in SOM^+ TRN neurons improved performance in the auditory/auditory task (Control, $n = 7$ mice, TRN KO, $n = 7$ mice, $F(1,12) = 31.69$; session 1, $****P < 0.0001$, session 2, $****P < 0.0001$, session 3, $***P = 0.0004$; Two-way repeated measures (RM) ANOVA followed by Bonferroni tests). (e & f) Selective deletion of *ErbB4* in SOM^+ TRN neurons impaired performance in the incongruent trials (e) (Control, $n = 7$ mice, TRN KO, $n = 7$ mice, $F(1,12) = 21.46$; session 1, $***P = 0.0001$, session 2, $**P = 0.006$, session 3, $**P = 0.001$, session 4, $**P = 0.002$, session 5, $*P = 0.013$, Two-way RM ANOVA followed by Bonferroni tests), but not in the congruent trials (f) ($F(1,12) = 0.06$; $P = 0.81$, Two-way RM ANOVA), of the visual/auditory task. Data are presented as mean \pm s.e.m.

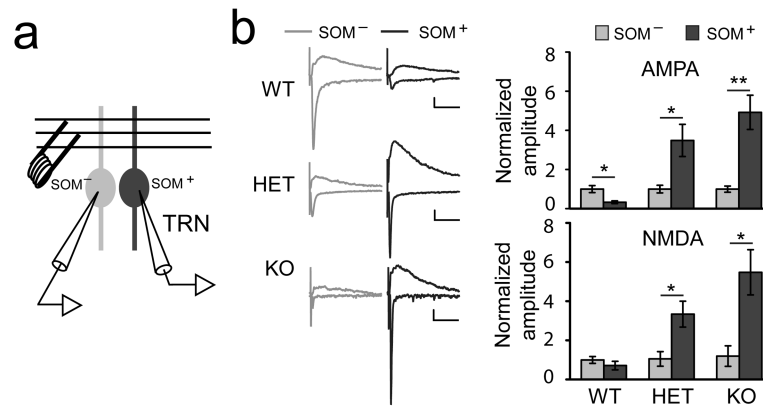


Figure 4. ErbB4 deficiency in SOM^+ TRN neurons enhances excitatory synaptic transmission onto these neurons

(a) A schematic of the paired-recording configuration. In red is a SOM^+ TRN neuron. (b) Left: representative EPSC traces recorded from SOM^-/SOM^+ neuronal pairs in the TRN in WT, HET, and KO mice. Calibrations: 20 pA and 50 ms. Right, top panel: quantification of AMPAR-mediated EPSC amplitude, which was normalized to the mean EPSC amplitude of SOM^- neurons (WT: SOM^- , 1 ± 0.18 , SOM^+ , 0.33 ± 0.07 , $n = 10$ pairs (7 mice), $DF = 9$, $T = 3.20$, $*P = 0.011$, paired t -test; HET: SOM^- , 1 ± 0.19 , SOM^+ , 3.48 ± 0.82 , $n = 7$ pairs (5 mice), $DF = 6$, $T = 2.71$, $*P = 0.035$, paired t -test; KO: SOM^- , 1 ± 0.16 , SOM^+ , 4.92 ± 0.88 , $n = 9$ pairs (5 mice), $DF = 8$, $T = 4.35$, $**P = 0.0024$, paired t -test). Bottom panel: quantification of NMDAR-mediated EPSC amplitude, which was normalized to the mean EPSC amplitude of SOM^- neurons (WT: SOM^- , 1 ± 0.18 , SOM^+ , 0.71 ± 0.22 , $n = 4$ pairs (4 mice), $DF = 3$, $T = 2.47$, $P = 0.09$, paired t -test; HET: SOM^- , 1 ± 0.37 , SOM^+ , 3.34 ± 0.66 , $n = 4$ pairs (3 mice), $DF = 3$, $T = 5.46$, $*P = 0.012$, paired t -test; KO: SOM^- , 1 ± 0.52 , SOM^+ , 5.48 ± 1.16 , $n = 5$ pairs (4 mice); $DF = 4$, $T = 3.40$, $*P = 0.027$, paired t -test). Data are presented as mean \pm s.e.m.

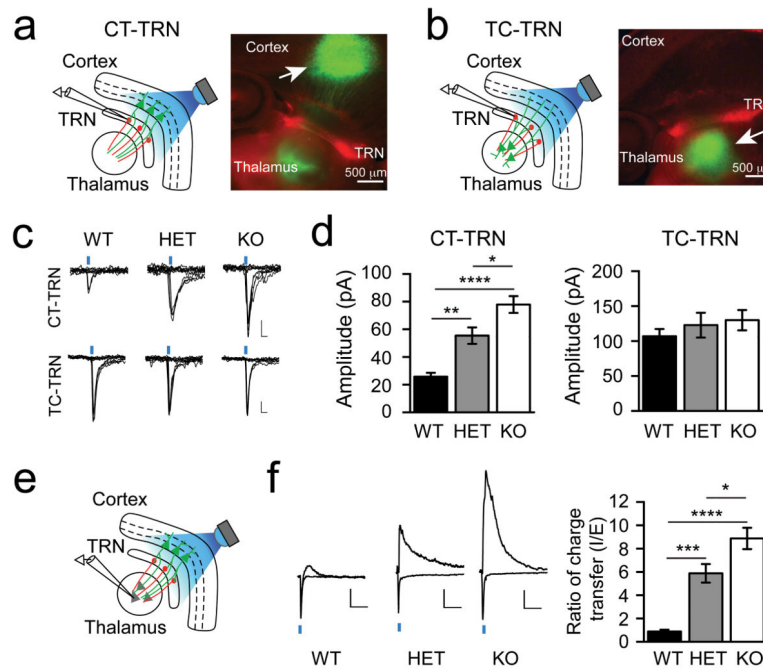


Figure 5. ErbB4 deficiency in SOM^+ TRN neurons selectively enhances cortical drive onto TRN

(a) Left: a schematic of the recording configuration. The CT-TRN pathway is selectively stimulated by photo-activation of Chr2 (green), and EPSCs are recorded from SOM^+ TRN neurons (red). Right: an image of a brain slice used in the recording. The slice was prepared from a *SOM-Cre;Ai14* mouse in which the AAV-CAG-ChR2(H134R)-YFP was injected into the primary somatosensory cortex (arrow). (b) Same as in a, except that the TC-TRN pathway was selectively stimulated, and the AAV-CAG-ChR2(H134R)-YFP was injected into the ventrobasal complex of the thalamus (arrow). (c) Representative emEPSC traces recorded from SOM^+ TRN neurons in response to the photo-stimulation (blue bars) of either the CT-TRN (top row) or the TC-TRN (bottom row) pathway, using the minimal photo-stimulation protocol. Calibrations: 20 pA and 2 ms. (d) Left: quantification of the amplitude of emEPSCs driven by the CT-TRN pathway (WT: 25.81 ± 7.35 pA, $n = 7$ cells (2 mice)); HET: 55.45 ± 5.91 pA, $n = 10$ cells (3 mice); KO: 77.92 ± 6.07 pA, $n = 8$ cells (3 mice); $F(2,22) = 20.23$, $*P = 0.018$, $**P = 0.0027$, $****P < 0.0001$, one-way ANOVA followed by Tukey's test). Right: quantification of the amplitude of emEPSCs driven by the TC-TRN pathway (WT: 106.8 ± 10.41 pA, $n = 10$ cells (3 mice)); HET: 122.8 ± 17.74 pA, $n = 9$ cells (2 mice); KO: 129.9 ± 14.53 pA, $n = 11$ cells (3 mice); $F(2,27) = 0.70$, $P = 0.5$, one-way ANOVA). (e) A schematic of the recording configuration, in which both the CT axons and their collaterals to TRN were photo-stimulated, and the synaptic responses were recorded from neurons in the thalamus. (f) Left: representative synaptic response traces recorded from thalamic neurons in response to photo-stimulation (blue bars) of the CT pathway. EPSCs and IPSCs in each neuron evoked by the same stimulation were recorded at the reversal potential of inhibitory and excitatory synaptic currents, respectively. Calibrations: 50 pA and 100 ms. Right: quantification of the ratio of inhibitory to excitatory charge transfer (I/E) (WT: 0.88 ± 0.15 , $n = 9$ cells (3 mice)); HET: 5.88 ± 0.79 , $n = 16$ cells (3 mice); KO: $8.87 \pm$

0.91, $n = 16$ cells (3 mice); $F(2,38) = 19.70$, $*P = 0.023$, $***P = 0.001$, $****P < 0.0001$, one-way ANOVA followed by Tukey's test). Data are presented as mean \pm s.e.m.

Author Manuscript

Author Manuscript

Author Manuscript

Author Manuscript

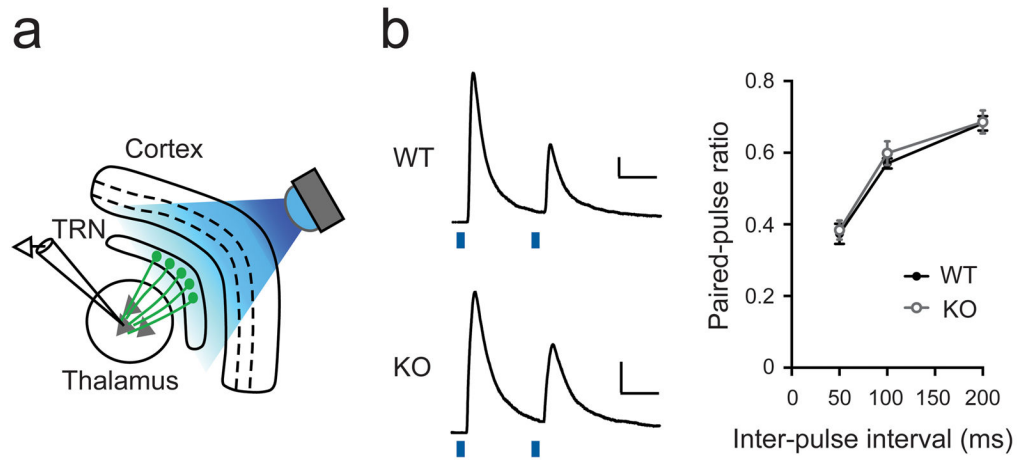


Figure 6. ErbB4 deficiency does not affect presynaptic function of SOM⁺ TRN neurons
(a) A schematic recording configuration. The SOM⁺ TRN neurons (green) in *SOM-IRE5-Cre* mice were infected with the AAV-DIO-ChR2(H134R)-YFP. The IPSCs, which were evoked by photo-stimulation of the SOM⁺ TRN neurons, were recorded from neurons in the thalamus. **(b)** Left: representative IPSC traces, which were recorded from a thalamic neuron in a *SOM^{ErbB4}^{+/+}* (WT; top) or a *SOM^{ErbB4}^{-/-}* (KO; bottom) mouse, respectively, in response to photo-stimulation (blue bars) of the SOM⁺ TRN neurons. A pair-pulse stimulation protocol was used. Calibrations: 50 pA and 50 ms. Right: there was no significant difference between WT and KO mice in the paired-pulse ratio at different inter-pulse intervals (WT, n = 11 cells; KO, n = 14 cells; $F(1,23) = 0.29$, $P = 0.59$, two-way RM ANOVA). Under our experimental regime there was no significant difference between WT and KO in the peak amplitude of the first IPSCs in the paired-pulses (WT, 240.1 ± 29.8 pA, n = 11; KO, 257.6 ± 39 pA, n = 15; $P = 0.74$, *t*-test). Data are presented as mean \pm s.e.m.

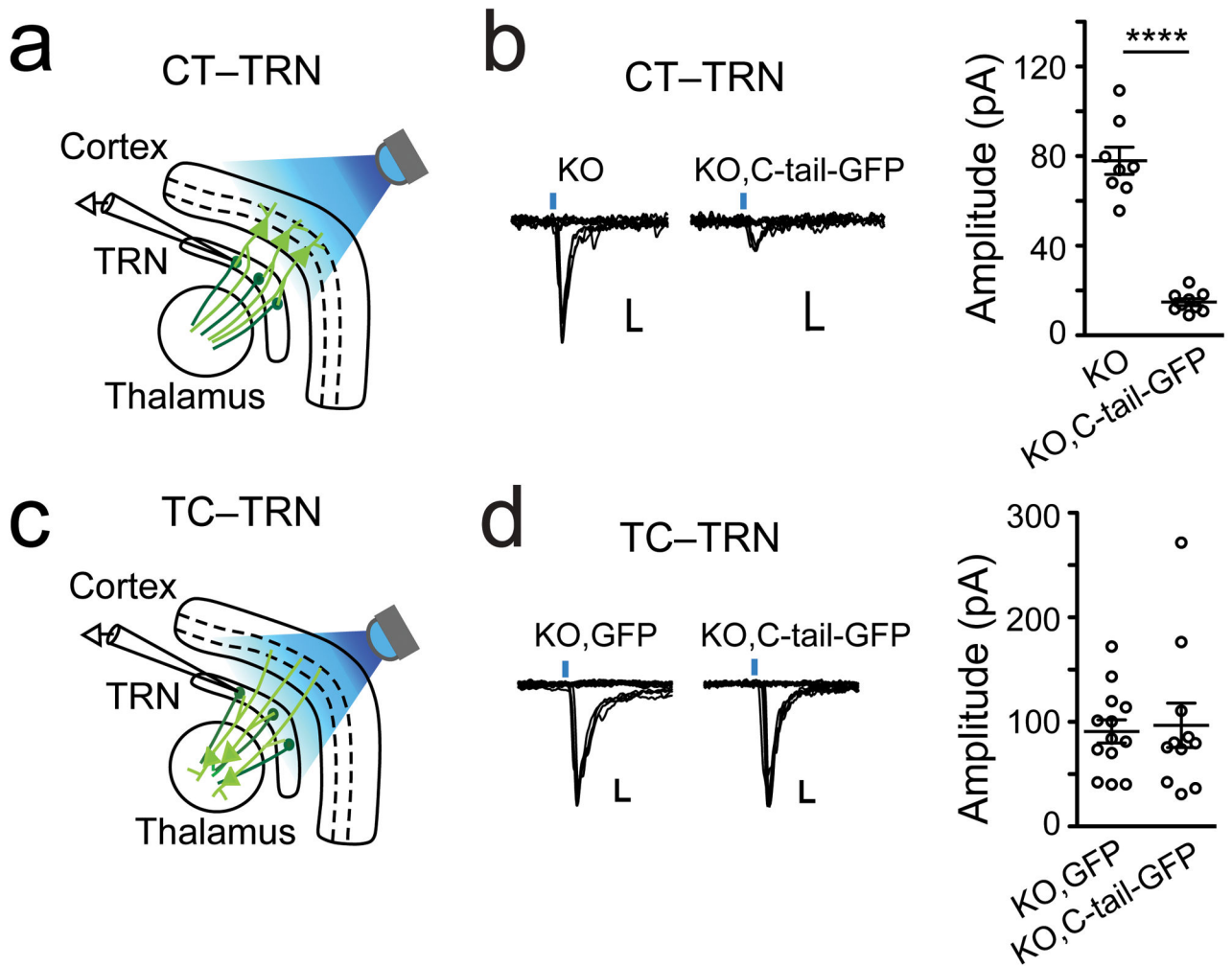


Figure 7. Blocking GluA4 trafficking in SOM^+ TRN neurons in *ErbB4* mutant mice reverses the enhanced cortical drive

(a) A schematic of the recording configuration. The CT-TRN pathway in $SOM^{ErbB4^{-/-}}$ (KO) mice is selectively stimulated by photo-activation of ChR2-YFP (light green), and EPSCs are recorded from SOM^+ TRN neurons (dark green). (b) Left: representative emEPSC traces recorded from a control SOM^+ TRN neuron (“KO”), and a SOM^+ TRN neuron expressing GluA4-C-tail-GFP (“KO, C-tail-GFP”). The emEPSCs were evoked by minimal photo-stimulation (blue bars) of the CT-TRN pathway. Calibrations: 20 pA and 2 ms. Right: quantification of the emEPSC amplitude (“KO”, $n = 8$ cells (2 mice)); “KO, C-tail-GFP”, $n = 9$ cells (3 mice); $DF = 15$; $T = 10.65$, **** $P < 0.0001$, t -test). The KO data is the same as that in Fig. 5c & d. (c) Same as in (a), except that the TC-TRN pathway is selectively stimulated. (d) Left: representative emEPSC traces recorded from a control SOM^+ TRN neuron expressing GFP (“KO, GFP”), and a SOM^+ TRN neuron expressing GluA4-C-tail-GFP (“KO, C-tail-GFP”). The emEPSCs were evoked by minimal photo-stimulation (blue bars) of the TC-TRN pathway. Calibrations: 20 pA and 2 ms. Right: quantification of the emEPSC amplitude (“KO, GFP”: $n = 13$ cells (3 mice)); “KO, C-tail-

GFP”, n = 11 cells (3 mice); DF = 22, T = 0.25, P = 0.81, t-test). Data are presented as mean \pm s.e.m.

Author Manuscript

Author Manuscript

Author Manuscript

Author Manuscript

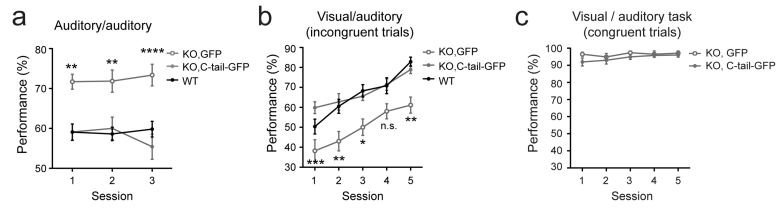


Figure 8. To rescue the behavioral phenotypes of ErbB4 mutant mice by reversing the enhanced cortical drive to TRN

(a) Expression of GluA4-C-tail in SOM^+ TRN neurons reduced the performance level of KO mice to that of WT in the auditory/auditory task (“KO, GFP”, $n = 8$ mice; “KO, C-tail-GFP”, $n = 8$ mice; $F(1,14) = 20.94$; session 1, $**P = 0.0042$, session 2, $**P = 0.0075$, session 3, $****P < 0.0001$, Two-way RM ANOVA followed by Bonferroni tests). The WT data in Fig. 3a is re-plotted here for visual inspection. (b & c) Expression of GluA4-C-tail in SOM^+ TRN neurons increased the performance of KO mice in the incongruent trials (b) (“KO, GFP”, $n = 8$ mice; “KO, C-tail-GFP”, $n = 8$ mice; $F(1,14) = 19.61$; session 1, $***P = 0.0007$, session 2, $**P = 0.0024$, session 3, $*P = 0.025$, session 4, n.s., not significant ($P = 0.074$), session 5, $**P = 0.0074$; Two-way RM ANOVA followed by Bonferroni tests), but not in the congruent trials (c) ($F(1,14) = 2.09$, $P = 0.17$, Two-way RM ANOVA), of the visual/auditory task. The WT data in Fig. 3b is re-plotted here for visual inspection. Data are presented as mean \pm s.e.m.